HHS Public Access

Author manuscript

Radiology. Author manuscript; available in PMC 2017 August 25.

Published in final edited form as:

Radiology. 2016 February ; 278(2): 536–545. doi:10.1148/radiol.2015150160.

Imaging Cerebral Microhemorrhages in Military Service Members with Chronic Traumatic Brain Injury

Wei Liu, DSc, **Karl Soderlund, MD**, **Justin S. Senseney, MS**, **David Joy, BS**, **Ping-Hong Yeh, PhD**, **John Ollinger, PhD**, **Elyssa B. Sham, BA**, **Tian Liu, PhD**, **Yi Wang, PhD**, **Terrence R. Oakes, PhD**, and **Gerard Riedy, MD, PhD**

[1]National Intrepid Center of Excellence (NICoE), Walter Reed National Military Medical Center, 4860 S Palmer Rd, Bethesda, MD 20889-5649 (W.L., K.S., J.S.S., D.J., P.H.Y., J.O., E.B.S., T.R.O., G.R.); Center for Neuroscience and Regenerative Medicine, Bethesda, Md (D.J., T.R.O., G.R.); The Henry M. Jackson Foundation for the Advancement of Military Medicine, Bethesda, Md (D.J.); Biomedical Engineering Department, Cornell University, New York, NY (T.L., Y.W.); and The NorthTide Group, Sterling, Va (W.L., E.B.S.)

Abstract

Purpose—To detect cerebral microhemorrhages in military service members with chronic traumatic brain injury by using susceptibility-weighted magnetic resonance (MR) imaging. The longitudinal evolution of microhemorrhages was monitored in a subset of patients by using quantitative susceptibility mapping.

Materials and Methods—The study was approved by the Walter Reed National Military Medical Center institutional review board and is compliant with HIPAA guidelines. All participants underwent two-dimensional conventional gradient-recalled-echo MR imaging and three-dimensional flow-compensated multi-echo gradient-recalled-echo MR imaging (processed to generate susceptibility-weighted images and quantitative susceptibility maps), and a subset of patients underwent follow-up imaging. Microhemorrhages were identified by two radiologists independently. Comparisons of microhemorrhage number, size, and magnetic susceptibility

Address correspondence to: G.R. (gerard.p.riedy.civ@mail.mil).

The views expressed in this manuscript are those of the authors and do not reflect the official policy of the U.S. Departments of the Army, Navy, or Air Force; U.S. Department of Defense; or U.S. Government.

Author contributions:

Guarantors of integrity of entire study, W.L., G.R.; study concepts/study design or data acquisition or data analysis/interpretation, all authors; manuscript drafting or manuscript revision for important intellectual content, all authors; approval of final version of submitted manuscript, all authors; agrees to ensure any questions related to the work are appropriately resolved, all authors; literature research, W.L., T.L., G.R.; clinical studies, W.L., K.S., J.S.S., P.H.Y., E.B.S., G.R.; experimental studies, W.L., K.S., T.L., Y.W., T.R.O., G.R.; statistical analysis, W.L., D.J., J.O., T.R.O.; and manuscript editing, W.L., K.S., P.H.Y., J.O., E.B.S., Y.W., T.R.O., G.R.

Disclosures of Conflicts of Interest: W.L. disclosed no relevant relationships. **K.S.** disclosed no relevant relationships. **J.S.S.** disclosed no relevant relationships. **D.J.** disclosed no relevant relationships. **P.H.Y.** disclosed no relevant relationships. **J.O.** disclosed no relevant relationships. **E.B.S.** disclosed no relevant relationships. **T.L.** Activities related to the present article: disclosed no relevant relationships. Activities not related to the present article: author received payment from MedImageMetric; author has a QSM patent. Other relationships: disclosed no relevant relationships. **Y.W.** Activities related to the present article: disclosed no relevant relationships. Activities not related to the present article: disclosed no relevant relationships. Other relationships: author has a QSM patent. **T.R.O.** disclosed no relevant relationships. **G.R.** disclosed no relevant relationships.

Online supplemental material is available for this article.

derived from quantitative susceptibility maps between baseline and follow-up imaging examinations were performed by using the paired *t* test.

Results—Among the 603 patients, cerebral microhemorrhages were identified in 43 patients, with six excluded for further analysis owing to artifacts. Seventy-seven percent (451 of 585) of the microhemorrhages on susceptibility-weighted images had a more conspicuous appearance than on gradient-recalled-echo images. Thirteen of the 37 patients underwent follow-up imaging examinations. In these patients, a smaller number of microhemorrhages were identified at follow-up imaging compared with baseline on quantitative susceptibility maps (mean ± standard deviation, 9.8 microhemorrhages ± 12.8 vs 13.7 microhemorrhages ± 16.6; $P = .019$). Quantitative susceptibility mapping–derived quantitative measures of microhemorrhages also decreased over time: −0.85 mm^3 per day ± 1.59 for total volume ($P = .039$) and −0.10 parts per billion per day ± 0.14 for mean magnetic susceptibility ($P = .016$).

Conclusion—The number of microhemorrhages and quantitative susceptibility mapping–derived quantitative measures of microhemorrhages all decreased over time, suggesting that hemosiderin products undergo continued, subtle evolution in the chronic stage.

Traumatic brain injury (TBI) is a leading cause of death and disability in young people at the most productive time of their lives (1). Each year, an estimated 1.5 million people in the United States sustain nonfatal TBI (2). It has been estimated that 10%–20% of military personnel deployed to Iraq and Afghanistan have experienced TBI, with most cases (80%) being mild (3). The damage to the brain from TBI has traditionally been grouped into primary and secondary injuries. Primary injuries, such as cerebral microhemorrhage (CMH), occur as a direct result of the traumatic impact. Primary traumatic injuries can trigger secondary insults by increasing the intracranial pressure, which leads to cerebral swelling, vasospasm, ischemia, infarction, and herniation. Characterization of CMH may help to explain clinical symptoms and characterize the severity of brain damage due to trauma.

Traditionally, T2*-weighted gradient-recalled-echo (GRE) magnetic resonance (MR) imaging has been the method of choice to detect CMH. The presence, number, distribution, and especially size of the round parenchymal signal voids have been used to characterize CMH burden (4,5). Susceptibility-weighted imaging (SWI) reinforces susceptibility effects by manipulating magnitude images with phase information (6) and therefore provides better sensitivity compared with GRE imaging (7–9). Quantitative susceptibility mapping (QSM) is used to estimate the underlying susceptibility distribution. This represents an intrinsic tissue property, is independent of data acquisition parameters, and should reflect the actual spatial extent of lesions (10–13). Liu et al demonstrated that the total susceptibility measurement of CMH is more consistent than the size measurement obtained over a large range of echo times (14). It has also been shown that QSM enables discrimination between diamagnetic and paramagnetic lesions (15). Moreover, because the magnetic susceptibility of an iron-containing lesion is related to the concentration of iron, QSM can be applied to noninvasively measure iron concentration in microhemorrhages and other lesions (16).

CMH is a common finding in patients with TBI at the acute stage (17–19). Blood products in the brain undergo a complex degradation process from oxyhemoglobin to hemosiderin over a period of several months. The ability to monitor the evolution of microhemorrhages

could provide important information regarding disease progression or recovery. In the present study, we characterized CMHs in military service members with chronic TBI by using SWI. The longitudinal evolution of microhemorrhages was monitored in a subset of the patients by using QSM.

Materials and Methods

Subjects

The study was approved by the Walter Reed National Military Medical Center institutional review board and is compliant with Health Insurance Portability and Accountability Act guidelines. Military service members were recruited between March 1, 2011, and November 14, 2013, after obtaining informed consent at the National Intrepid Center of Excellence, Walter Reed National Military Medical Center, Bethesda, Maryland. Inclusion criteria included clinical diagnosis of TBI, active duty or Defense Enrollment Eligibility Reporting System eligible individuals, men and women between the ages of 18 and 60 years, and women who were not pregnant or breast feeding. Exclusion criteria were patients with TBI who were unable to consent to the study, those who were actively enrolled in other treatment trials with which this study would interfere, a history of prior severe neurological or psychiatric conditions, and metal implants or shrapnel. All participants (n = 603) underwent imaging with an extended MR imaging protocol. Figure 1 is a diagram of the patient population recruitment and exclusion. The subjects with TBI had predominantly chronic TBI (median time to MR imaging, 856 days after injury) and mild TBI (92.7%, 559 of 603 subjects). Forty-three patients (7.1%, 43 of 603) were identified who had at least one CMH. Six of the patients were excluded because of severe susceptibility or motion artifacts, leaving a total of 37 patients included in the conspicuity analysis. A subset of the patients (n = 55) returned for follow-up imaging. CMH was identified in 13 of the 55 patients with follow-up images. Table 1 summarizes the demographics of these patients. For patients who underwent multiple follow-up imaging examinations, the statistics were based on their first follow-up imaging examination findings. For patients who underwent follow-up imaging, multivitamins, pain relievers, antidepression medications, anti-inflammatory medications, and laxatives were the most common medications that were taken at the time of MR imaging.

Data Acquisition

The protocol included high-spatial-resolution anatomic T1-weighted imaging, T2-weighted imaging, and T2-weighted fluid-attenuated inversion-recovery imaging; four functional MR imaging sequences; diffusion-tensor imaging; perfusion imaging with dynamic susceptibility contrast material–enhanced imaging; spectroscopic imaging; and GRE and multiecho gradient-echo imaging. Images were acquired with a 3-T whole-body MR imaging unit (Discovery MR750; GE Healthcare, Milwaukee, Wis) equipped with a 32-channel phased-array head coil (MR Instruments; Minneapolis, Minn). GRE images were acquired by using a two-dimensional gradient-echo sequence with a repetition time (msec)/echo time (msec) of 550/30, flip angle of 20°, field of view of 24 × 24 cm, matrix of 288 × 192, and 45 sections acquired with 3-mm thickness. The images used for SWI and QSM were acquired by using a three-dimensional flow-compensated multiecho gradient-echo sequence with a repetition

time of 45 msec, a total of five echoes (time of the first echo, 13 msec) with echo spacing of 6 msec, flip angle of 20°, field of view of 24 × 24 cm, matrix of 512 × 256, and 88 sections acquired with 1.5-mm thickness.

Data Reconstruction

SWI images were processed from the magnitude and phase images of the third echo (echo time of 25 msec) by using custom software (6). QSM images were calculated from the real and imaginary data by using the morphology-enabled dipole inversion, or MEDI, approach (11,14), which was implemented as part of the MEDI software (T.L. holds a patent [no. US20130221961 A1], which refers to the MEDI reconstruction method used for reconstructing QSM images). All five echoes were used to generate the QSM images. Minimum (SWI) and maximum (QSM) intensity projections were generated over five adjacent sections (7.5 mm thick).

The reconstructed SWI and QSM images, together with GRE images, were sent to a picture archiving and communication system (Agfa Health-care, Mortsel, Belgium) for radiologic interpretation. CMH was identified by two radiologists independently (G.R., with 16 years of experience; and K.S., with 3 years of experience) on GRE, SWI, and QSM images. The reported CMH represents the consensus between the two radiologists. The conspicuity of the CMH at SWI was scored relative to the appearance on the conventional GRE images by one radiologist (K.S.) using the following criteria: appearance less conspicuous than that on GRE images, appearance equivalent to that on GRE images, and appearance more conspicuous than that on GRE images. κ analysis was performed to assess the interobserver reliability between the two radiologists.

For patients who underwent follow-up imaging, QSM images were transferred to a Mac Pro desktop computer (Apple, Cupertino, Calif). Manual segmentation was performed on QSM images by an MR imaging data analyst (W.L., with 15 years of experience) for each lesion using Analysis of Functional NeuroImages software (AFNI, National Institute for Mental Health, Bethesda, Md) (20). The volume of the lesion, mean magnetic susceptibility, and total magnetic susceptibility were determined on the basis of the manually depicted regions of interest. The comparison between baseline and follow-up imaging findings was performed by using a paired *t* test. A one-sample *t* test was used to assess the changes identified between baseline images and follow-up images. The Pearson correlation coefficient was used to assess the changes between total volume and mean magnetic susceptibility of CMH.

Results

The two radiologists agreed on findings in 41 of 43 patients with microhemorrhages. The interobserver reliability was 96.4% according to κ analysis. Figure 2 contains representative SWI, GRE, and QSM images in a patient with TBI. The arrows indicate a CMH that is visible on SWI, GRE, and QSM images. Magnetic susceptibility from blood products presented in the lesion yields the hypointensity at GRE imaging and SWI. In contrast, this lesion appears hyperintense on QSM images, representing higher magnetic susceptibility

compared with its surroundings. The arrowheads indicate a CMH that is visible on the SWI and QSM images but not on the GRE image.

On SWI images, 585 microhemorrhages were detected in 37 patients, compared with 362 microhemorrhages detected on GRE images. Significantly more CMHs were detected with SWI compared with GRE imaging for individual patients (mean ± standard deviation, 17.7 CMHs ± 20.7 vs 11.0 CMHs ± 12.6; $P < .001$). All microhemorrhages were scored as more conspicuous or equally conspicuous at SWI compared with GRE imaging. In fact, most micro-hemorrhages (451 of 585, 77%) at SWI appeared more conspicuous than on GRE images (Fig E1 [online]). Figure 3 illustrates the distribution of the microhemorrhages detected with SWI in the cerebral hemispheres. Frontal subcortical regions exhibited the most occurrences, with 101 microhemorrhages on the left side and 73 microhemorrhages on the right side, for a combined total of 30% (174 of 585) of detected microhemorrhages. The second most affected region was the parietal subcortical region, with 15% of the total microhemorrhages (87 of 585 microhemorrhages, 41 on the right and 46 on the left), followed by the temporal subcortical region, with 14% of the total microhemorrhages (79 of 585 microhemorrhages, 48 on the right and 31 on the left).

When patients were classified into four groups on the basis of time since injury, the occurrence of CMH in patients who underwent imaging more than 1 year after injury was much lower than those who underwent imaging at earlier stages: 5.2% (24 of 461 patients) versus 24% (six of 25 patients) in patients who underwent imaging less than 3 months after injury, 18.4% (seven of 38 patients) in patients who underwent imaging 3–6 months after injury, and 7.6% (six of 79 patients) in patients who underwent imaging 6–12 months after injury, respectively (Table 2). Statistical data for patients with mild TBI are presented in Table E1 (online).

Figure 4 illustrates a cluster of microhemorrhages in a patient who underwent imaging 6 months, 12 months, and 36 months after injury. It is obvious that the number of microhemorrhages in this cluster decreased dramatically over time. The evolution of microhemorrhages in two other patients is presented in Figures E2 and E3 (online). Among the 13 patients, the total number of microhemorrhages decreased in 11 patients at SWI and in 10 patients at QSM (Table 3). The number of CMHs detected decreased significantly from baseline to follow-up imaging for both measurements ($P = .013$ for SWI and $P = .019$ for QSM).

QSM-derived total volume and mean magnetic susceptibility of individual patients both decreased significantly from baseline to follow-up imaging ($P = .042$ for total volume [Fig 5, *A*], $P = .009$ for mean magnetic susceptibility [Fig 5, *E*]). The total magnetic susceptibility showed a trend toward decreasing from baseline to follow-up imaging ($P = .078$, Fig 5, *C*). Figure 5, *B, D*, and *F*, illustrate the changes in the total volume of microhemorrhages, total magnetic susceptibility, and mean magnetic susceptibility (from baseline to follow-up imaging), respectively, for each individual patient. The negative bars demonstrated that the total volume of microhemorrhages decreased in all 13 patients (Fig 5, *B*). In all but two patients, the total magnetic susceptibility of individual patients decreased at follow-up imaging compared with baseline (Fig 5, *D*), while the mean magnetic susceptibility also

decreased in another 11 patients. Two of the patients, however, demonstrated slightly increased mean magnetic susceptibility (Fig 5, *F*).

In Figure 6, the changes in total volume are plotted (Fig 6, *A*), along with total magnetic susceptibility (Fig 6, *B*) and mean magnetic susceptibility (Fig 6, *C*) of individual patients versus time between follow-up and baseline imaging. The rate of changes in terms of CMH volume, total magnetic susceptibility, and mean magnetic susceptibility is shown in Table 4. The rate of changes was −0.85 mm^3 per day ± 1.59 for total volume ($P = .039$), −238 ppb per day ± 506 for total magnetic susceptibility ($P = .058$), and −0.10 ppb per day ± 0.14 for mean susceptibility ($P = .016$). No significant correlation was observed between the changes in total volume and mean magnetic susceptibility ($r = -0.053$, $P = .864$).

Discussion

The current study demonstrated that SWI was used to detect a higher number of microhemorrhages in military patients with TBI and exhibited better conspicuity compared with conventional GRE imaging. Even though previous studies have shown that SWI is superior to GRE in the detection of hemorrhage (17–19), its clinical application in military clinics is still limited. Our results indicate that for the identification of the presence or absence of CMHs, SWI should be the method of choice clinically.

In a subset of patients who underwent follow-up imaging, quantitative measurements of microhemorrhages derived from QSM decreased over time. Aging of the hemorrhagic lesion is largely an unsolved issue. Zhang et al observed that the magnetic susceptibility of thrombus changed from strongly paramagnetic to slightly diamagnetic at the hyperacute stage by using an in vitro flow-driven thrombus model (21). We showed, for the first time to our knowledge, the longitudinal evolution of CMH in the chronic stage. Conventional teaching holds that the brain has no mechanism to remove hemosiderin once it is formed, and it is therefore present in the brain for the rest of one’s life as a marker of prior hemorrhage. Our results, however, demonstrated that not only the total number of microhemorrhages decreased from baseline to follow-up imaging, but quantitative measurements, such as total volume of microhemorrhages and mean magnetic susceptibility, also decreased over time. In a recent study, investigators reported that the magnetic susceptibilities of multiple sclerosis lesions relative to normal-appearing white matter were higher for early to intermediately aged nonenhanced lesions than for chronic nonenhanced lesions (22). Since iron is the major contributor to the magnetic susceptibility in both CMH and multiple sclerosis lesions, both results suggest that the iron concentration in brain lesions continues a chronic, subtle evolution, even in the chronic stage.

The incidence of CMH in this TBI population was lower than initially anticipated. In our military subject population, most of the traumatic injuries occurred in theater (an area where warfare events occur), where there is no access to MR imaging in the acute phase. The median time to MR imaging for our subject population was 856 days after injury. However, the percentage of patients with identified microhemorrhages increased dramatically when MR imaging was performed closer to the injury date. Microhemorrhages were identified in 24% of the patients who underwent imaging within 3 months after injury and in 18.4% of

patients who underwent imaging 3–6 months after injury. This finding is consistent with previous studies of TBI in civilian populations that demonstrated higher incidences of central nervous system hemorrhage in the acute or subacute time frame (17–19). The percentages of patients with moderate to severe TBI were similar for groups who underwent imaging 3–6 months (four of 38 patients, 10.5%) and 6–12 months (11 of 79 patients, 13.9%) after injury. However, the incidence of CMH was much lower in the 6–12-month group (7.6% vs 18.4%), suggesting that the injury severity in these patients was not the primary cause for this observation. The low incidence of TBI-related CMH in the chronic TBI population and higher incidence of TBI-related CMH at earlier stages of TBI could be related to evolution of the blood products over time.

There are some limitations in the current study. The volume assessment of the CMH lesions was performed manually. Owing to the small size of the lesions, this process might be prone to measurement errors. In the longitudinal study, the region of interest drawing was not completely blinded to the longitudinal time point, since this was a 2-year study and some of the baseline images were already analyzed prior to follow-up image analysis. Because iron in microhemorrhage is the most concentrated in the center, the smaller the volume drawn, the larger the mean susceptibility. Therefore, the volume of the CMH is negatively correlated with the mean magnetic susceptibility for a specific lesion. Our results demonstrated that both the size and mean magnetic susceptibility of CMH decreased over time. Therefore, it is unlikely that a subjective bias toward later imaging examinations caused the results. Nevertheless, this study was a retrospective study from a larger research project. All patients underwent a prolonged neuroimaging protocol to apply state-of-the-art MR imaging techniques in the investigation of TBI. The multiecho images used for SWI and QSM analysis were acquired near the end of the 90-minute examination. As a result, some images were subject to moderate motion artifacts. This was especially pronounced in the follow-up imaging examination of one patient, which may explain why the mean magnetic susceptibility of a patient increased at the follow-up imaging examination, even though it was pointed out by the radiologist (G.R.) that this lesion was less conspicuous at follow-up imaging.

In summary, in the current study we found that the number of microhemorrhages and QSM-derived measurements of microhemorrhages all decreased over time, suggesting that hemosiderin products undergo continued, subtle evolution in the chronic stage of TBI. However, our study included a limited number of patients who underwent follow-up imaging examinations. In future studies, this method will need to be replicated in a larger patient population. Furthermore, by correlating microhemorrhages with regional brain volumes, abnormalities such as fiber discontinuities or hyperintensities on T2-weighted fluid attenuation inversion-recovery images will facilitate the investigation of this disease.

Supplementary Material

Refer to Web version on PubMed Central for supplementary material.

Acknowledgments

Supported by Center for Neuroscience and Regenerative Medicine grant no. 300606 and Congressionally Directed Medical Research Programs grant no. PT074437.

Abbreviations

CMH	cerebral microhemorrhage
GRE	gradient-recalled-echo
ppb	parts per billion
QSM	quantitative susceptibility mapping
SWI	susceptibility-weighted imaging
TBI	traumatic brain injury

References

1. Report to Congress on mild traumatic brain injury in the United States: steps to prevent a serious public health problem. National Center for Injury Prevention and Control, Centers for Disease Control and Prevention; http://www.cdc.gov/traumaticbraininjury/pdf/mtbireport-a.pdf. Published September 2003 [Accessed July 30, 2015]
2. Sosin DM, Sniezek JE, Thurman DJ. Incidence of mild and moderate brain injury in the United States, 1991. Brain Inj. 1996; 10(1):47–54. [PubMed: 8680392]
3. Warden D. Military TBI during the Iraq and Afghanistan wars. J Head Trauma Rehabil. 2006; 21(5): 398–402. [PubMed: 16983225]
4. Xi G, Keep RF, Hoff JT. Mechanisms of brain injury after intracerebral haemorrhage. Lancet Neurol. 2006; 5(1):53–63. [PubMed: 16361023]
5. Greenberg SM, Vernooij MW, Cordonnier C, et al. Cerebral microbleeds: a guide to detection and interpretation. Lancet Neurol. 2009; 8(2):165–174. [PubMed: 19161908]
6. Haacke EM, Xu Y, Cheng YC, Reichenbach JR. Susceptibility weighted imaging (SWI). Magn Reson Med. 2004; 52(3):612–618. [PubMed: 15334582]
7. Tong KA, Ashwal S, Holshouser BA, et al. Hemorrhagic shearing lesions in children and adolescents with posttraumatic diffuse axonal injury: improved detection and initial results. Radiology. 2003; 227(2):332–339. [PubMed: 12732694]
8. Mori N, Miki Y, Kikuta K, et al. Microbleeds in moyamoya disease: susceptibility-weighted imaging versus $T2^*$-weighted imaging at 3 Tesla. Invest Radiol. 2008; 43(8):574–579. [PubMed: 18648257]
9. Nandigam RN, Viswanathan A, Delgado P, et al. MR imaging detection of cerebral microbleeds: effect of susceptibility-weighted imaging, section thickness, and field strength. AJNR Am J Neuroradiol. 2009; 30(2):338–343. [PubMed: 19001544]
10. Haacke EM, Tang J, Neelavalli J, Cheng YC. Susceptibility mapping as a means to visualize veins and quantify oxygen saturation. J Magn Reson Imaging. 2010; 32(3):663–676. [PubMed: 20815065]
11. Liu T, Liu J, de Rochefort L, et al. Morphology enabled dipole inversion (MEDI) from a single-angle acquisition: comparison with COSMOS in human brain imaging. Magn Reson Med. 2011; 66(3):777–783. [PubMed: 21465541]
12. Schweser F, Sommer K, Deistung A, Reichenbach JR. Quantitative susceptibility mapping for investigating subtle susceptibility variations in the human brain. Neuroimage. 2012; 62(3):2083–2100. [PubMed: 22659482]

13. Neelavalli J, Cheng YC, Jiang J, Haacke EM. Removing background phase variations in susceptibility-weighted imaging using a fast, forward-field calculation. J Magn Reson Imaging. 2009; 29(4):937–948. [PubMed: 19306433]
14. Liu T, Surapaneni K, Lou M, Cheng L, Spincemaille P, Wang Y. Cerebral micro-bleeds: burden assessment by using quantitative susceptibility mapping. Radiology. 2012; 262(1):269–278. [PubMed: 22056688]
15. Schweser F, Deistung A, Lehr BW, Reichenbach JR. Differentiation between diamagnetic and paramagnetic cerebral lesions based on magnetic susceptibility mapping. Med Phys. 2010; 37(10): 5165–5178. [PubMed: 21089750]
16. Zheng W, Nichol H, Liu S, Cheng YC, Haacke EM. Measuring iron in the brain using quantitative susceptibility mapping and X-ray fluorescence imaging. Neuroimage. 2013; 78:68–74. [PubMed: 23591072]
17. Wu Z, Li S, Lei J, An D, Haacke EM. Evaluation of traumatic subarachnoid hemorrhage using susceptibility-weighted imaging. AJNR Am J Neuroradiol. 2010; 31(7):1302–1310. [PubMed: 20190211]
18. Roberts I, Yates D, Sandercock P, et al. Effect of intravenous corticosteroids on death within 14 days in 10008 adults with clinically significant head injury (MRC CRASH trial): randomised placebo-controlled trial. Lancet. 2004; 364(9442):1321–1328. [PubMed: 15474134]
19. Perel P, Roberts I, Bouamra O, Woodford M, Mooney J, Lecky F. Intracranial bleeding in patients with traumatic brain injury: a prognostic study. BMC Emerg Med. 2009; 9:15. [PubMed: 19650902]
20. Cox RW. AFNI: software for analysis and visualization of functional magnetic resonance neuroimages. Comput Biomed Res. 1996; 29(3):162–173. [PubMed: 8812068]
21. Zhang, J., Nguyen, TD., Candela, XJ., Witmer, KP., Manning, KB., Wang, Y. Quantitative relaxation time and susceptibility mapping of thrombus [abstr]. Proceedings of the Twenty-Second Meeting of the International Society for Magnetic Resonance in Medicine; Berkeley, Calif: International Society for Magnetic Resonance in Medicine; 2014. p. 0112
22. Chen W, Gauthier SA, Gupta A, et al. Quantitative susceptibility mapping of multiple sclerosis lesions at various ages. Radiology. 2014; 271(1):183–192. [PubMed: 24475808]

Advances in Knowledge

- Patients with traumatic brain injury (TBI) showed a reduced number of cerebral microhemorrhages (CMHs) at follow-up compared with baseline images (mean ± standard deviation, 9.8 microhemorrhages ± 12.8 vs 13.7 microhemorrhages ± 16.6; $P = .019$).
- The total volume and mean magnetic susceptibility of the CMHs in patients with TBI both decreased over time: −0.85 mm^3 per day ± 1.59 for total volume ($P = .039$) and −0.10 parts per billion per day ± 0.14 for mean magnetic susceptibility ($P = .016$).
- The results suggest that hemosiderin products undergo continued, subtle evolution in the chronic stage of traumatic brain injury.

Implication for Patient Care

- Performing MR imaging in patients with TBI as early as possible would facilitate better evaluation of CMHs.

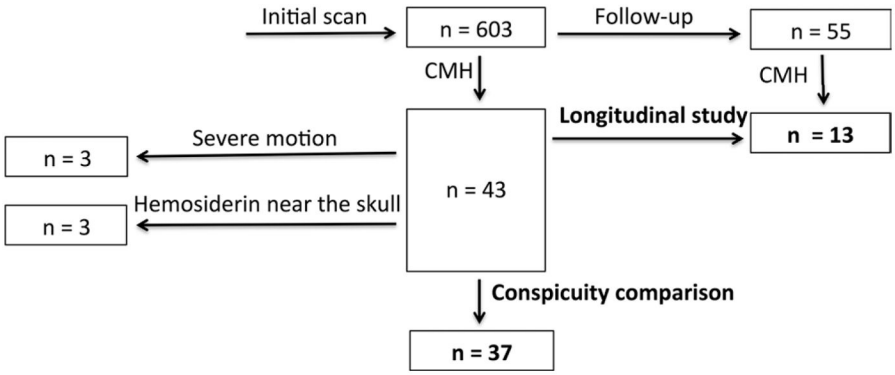

Figure 1.
Diagram of patient population recruitment and exclusion.

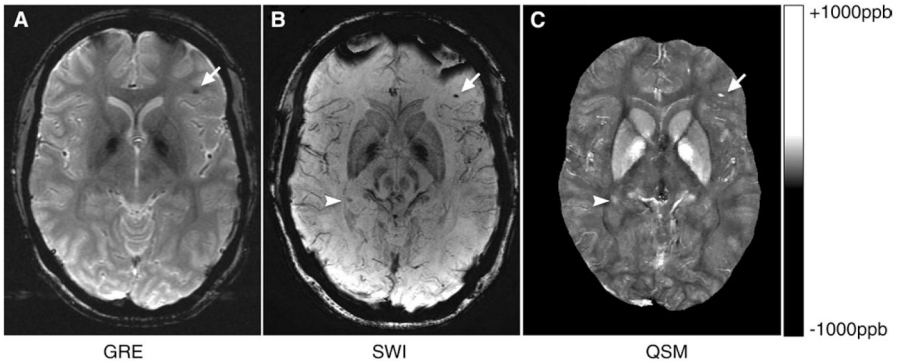

Figure 2.

A, GRE, *B,* SWI, and, *C,* QSM images in a patient with TBI. The arrows indicate a CMH that is visible on SWI, GRE, and QSM images. The arrowheads indicate another CMH that is visible on SWI and QSM images, but not the GRE image. *ppb* = parts per billion.

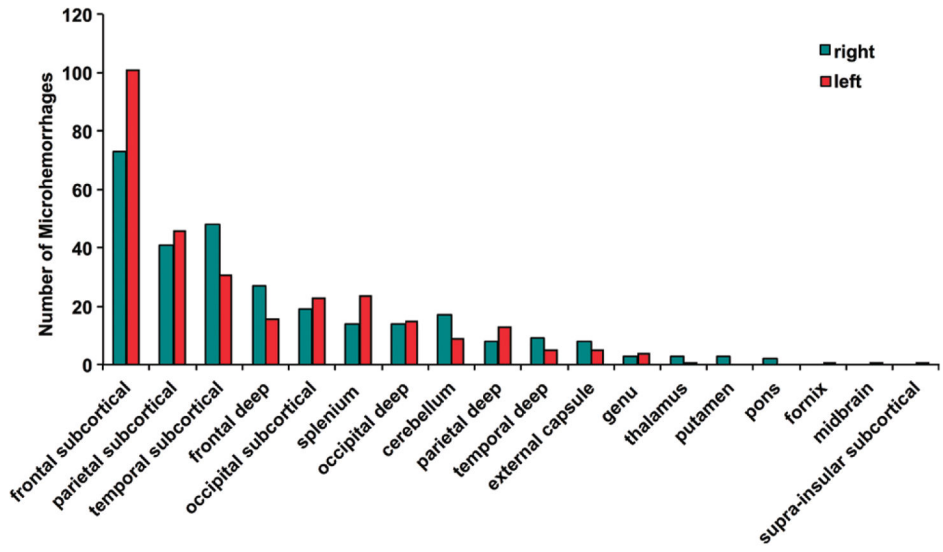

Figure 3.

Bar graph shows the distribution of the microhemorrhages in the cerebral hemispheres detected with SWI.

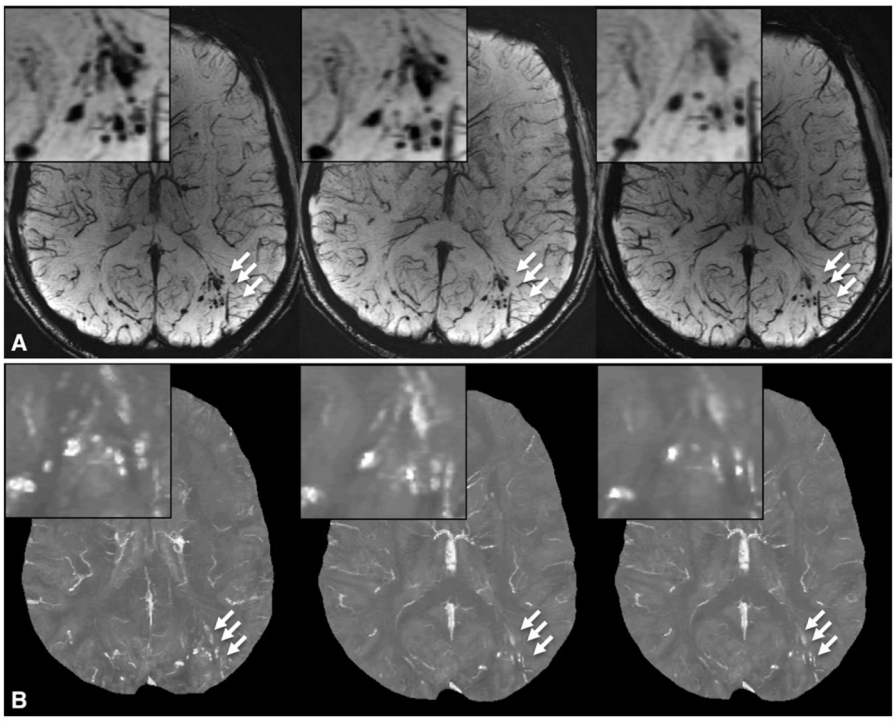

Figure 4.

A, SWI and, *B,* QSM images show the evolution of microhemorrhages (arrows) in a patient who underwent follow-up imaging.

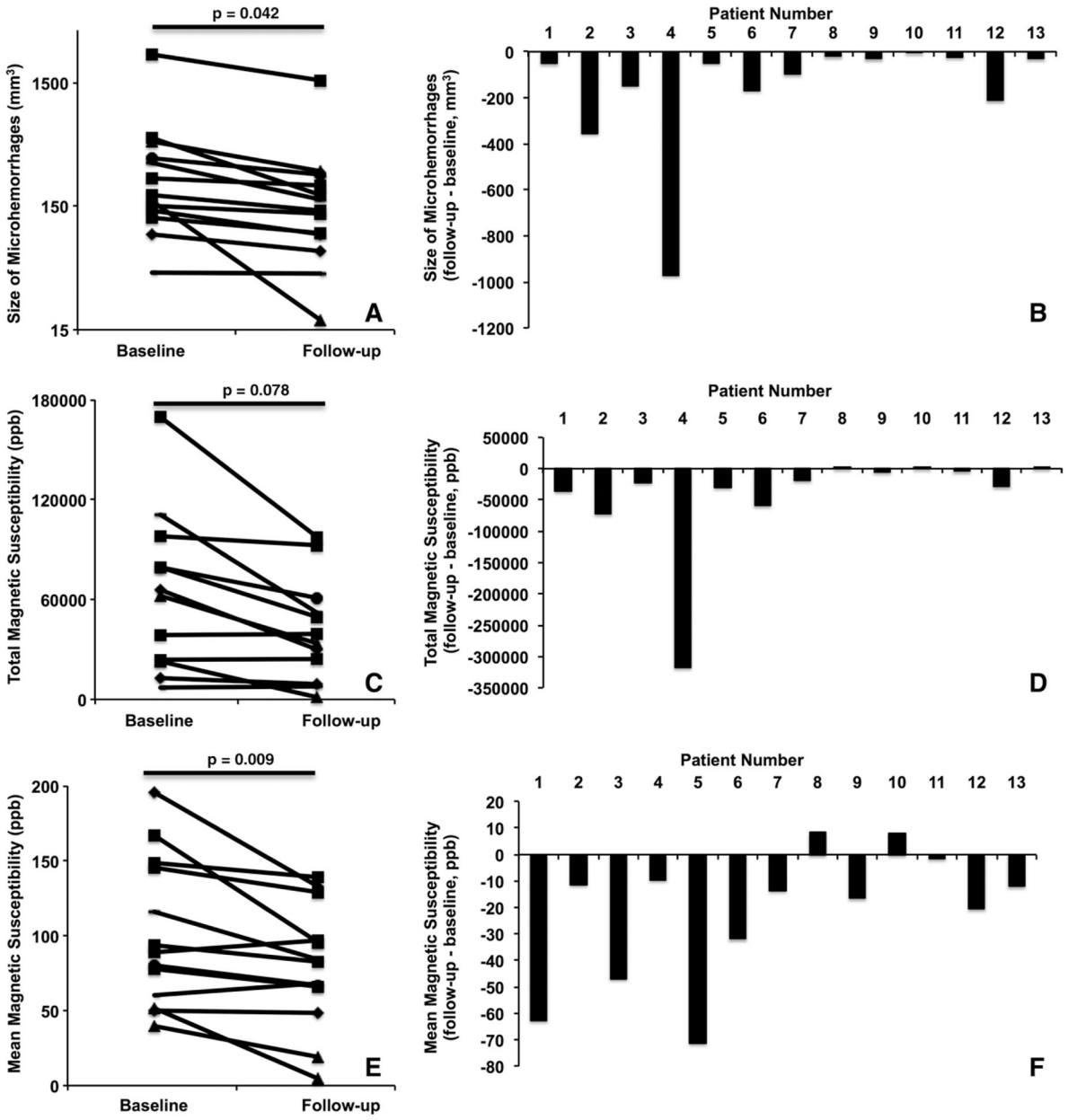

Figure 5.

A, Plot of the total volume of microhemorrhages in individual patients who underwent follow-up imaging. *B,* Bar graph shows the changes in total volume of microhemorrhages (from baseline to follow-up imaging) in individual patients. *C,* Plot of the total magnetic susceptibility of microhemorrhages in individual patients who underwent follow-up imaging. *D,* Bar graph of the changes in total magnetic susceptibility of microhemorrhages (from baseline to follow-up imaging) in individual patients. *E,* Plot of the mean magnetic susceptibility of microhemorrhages in individual patients who underwent follow-up imaging. *F,* Bar graph of the changes in mean magnetic susceptibility of microhemorrhages (from baseline to follow-up imaging) in individual patients.

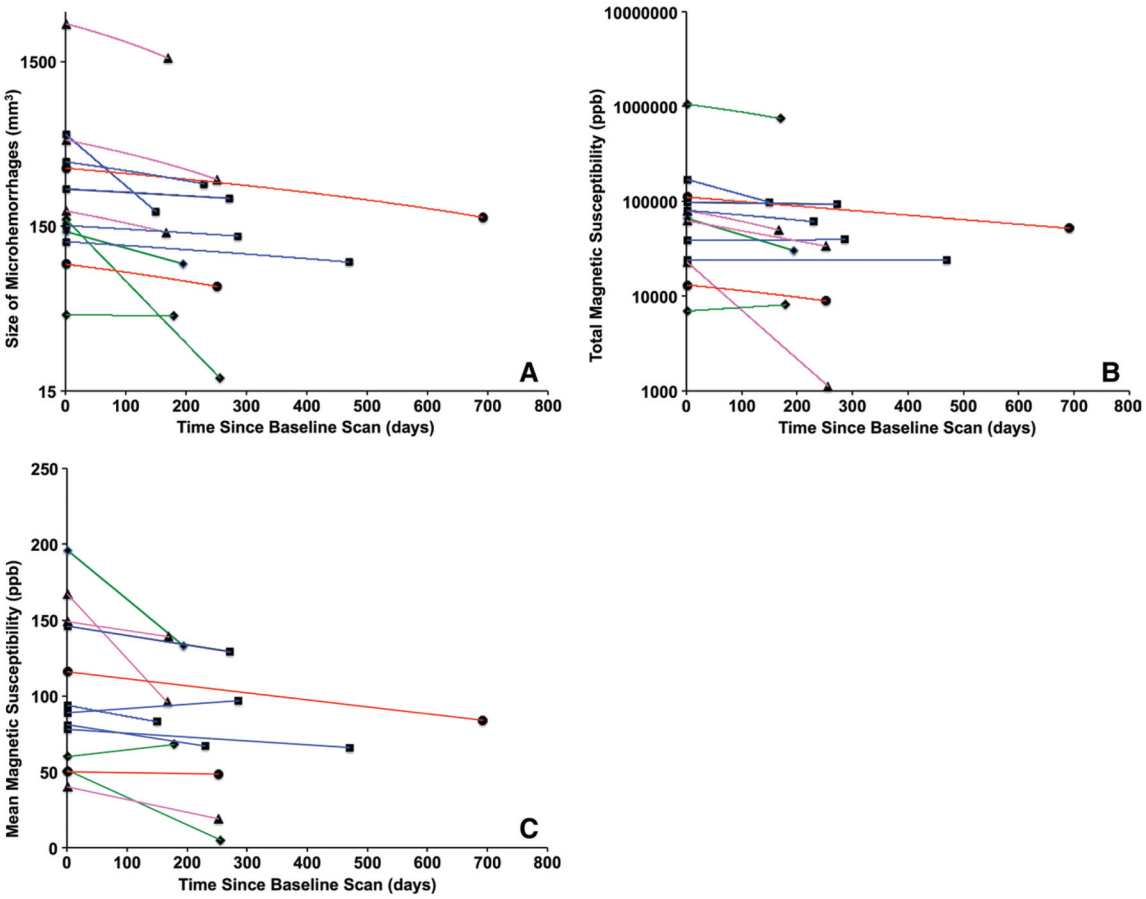

Figure 6.

Plots of the changes in, *A,* total volume, *B,* total magnetic susceptibility, and, *C,* mean magnetic susceptibility of microhemorrhages in individual patients versus the time between baseline and follow-up imaging examinations. The lines between baseline and follow-up imaging examinations are color coded on the basis of the time since injury at baseline MR imaging: Blue indicates less than 3 months, green indicates 3–6 months, purple indicates 6–12 months, and red indicates more than 1 year.

Table 1

Demographics of All Participants

Parameter	All Patients	Patients with CMH	Patients with CMH Who Underwent Follow-up Imaging
No. of subjects	603	37	13
No. of women	22 (3.6)	2 (5.4)	1 (7.7)
Mean age (y) *	33.8 ± 8.0 (33)	31.4 ± 7.4 (30)	29.8 ± 8.6 (29)
Time since injury at baseline imaging (d) *	1325 ± 1406 (856)	885 ± 1161 (386)	205 ± 226 (128)
Time between baseline and follow-up imaging (d) *	…	…	270 ± 144 (252)
No. of patients with blast injury	486 (80.6)	25 (67.6)	7 (53.8)
No. of patients with non–blast injury	117 (19.4)	12 (32.4)	6 (46.2)
No. of patients with severe TBI	9 (1.5)	7 (18.9)	3 (23.1)
No. of patients with moderate TBI	35 (5.8)	12 (32.4)	7 (53.8)
No. of patients with mild TBI	559 (92.7)	18 (48.6)	3 (23.1)

Note.—Frequencies are reported for categorical variables. Unless indicated otherwise, numbers in parentheses are percentages.

* Numbers are continuous variables, with data given as mean ± standard deviations and median values in parentheses.

Table 2

Incidence of CMH in Patient Groups Who Underwent Imaging at Different Times Since Injury

Time Since Injury	All Participants	Patients with CMH	Percentage of Patients with CMH
<3 mo	25 (8)	6	24.0
3–6 mo	38 (4)	7	18.4
6–12 mo	79 (11)	6	7.6
>1 y	461 (21)	24	5.2
Total	603 (44)	43	7.1

Note.—The numbers of patients with moderate to severe TBI are in parentheses.

Table 3

Number of CMHs Detected at Baseline and Follow-up Imaging

	No. of CMHs at SWI		No. of CMHs at QSM	
Patient No.	**Baseline**	**Follow-up**	**Baseline**	**Follow-up**
1	6	3	3	3
2	18	10	17	9
3	14	3	11	1
4	73	59	62	49
5	4	3	4	3
6	14	12	11	10
7	14	13	14	13
8	7	6	6	5
9	1	1	1	1
10	13	12	11	10
11	2	2	2	2
12	45	21	31	18
13	15	4	5	4
Mean*	17.4 ± 20.1	11.5 ± 15.4†	13.7 ± 16.6	9.8 ± 12.8‡

*Data are means ± standard deviations.

†$P = .013$.

‡$P = .019$.

Table 4

Changes in CMHs in Terms of Volume, Total Magnetic Susceptibility, and Mean Magnetic Susceptibility from Baseline to Follow-up Imaging

Patient No.	Changes in CMH Volume (mm^3 per day)	Changes in CMH Total Magnetic Susceptibility (ppb per day)	Changes in CMH Mean Magnetic Susceptibility (ppb per day)
1	−0.26	−182	−0.32
2	−2.36	−480	−0.08
3	−0.57	−85	−0.18
4	−5.71	−1866	−0.06
5	−0.28	−178	−0.43
6	−0.24	−84	−0.05
7	−0.42	−81	−0.06
8	−0.07	3	0.03
9	−0.11	−19	−0.06
10	−0.01	6	0.05
11	−0.09	−17	−0.01
12	−0.84	−114	−0.08
13	−0.07	1.1	−0.03
Mean *	−0.85 ± 1.59 †	−238 ± 506 ‡	−0.10 ± 0.14 §

* Data are means ± standard deviations.

† $P = .039$.

‡ $P = .058$.

§ $P = .016$.